Pockels effect in CVD-grown monolayer MoS_2

Masaki Tanabe[1], Ritsuki Okukawa[2], Tomoyuki Yokouchi[3], Yasumitsu Miyata[2,4], and Yuki Shiomi[1]

[1] Department of Basic Science, The University of Tokyo, Tokyo 153-8902, Japan
[2] Department of Physics, Tokyo Metropolitan University, Tokyo 192-0397, Japan
[3] RIKEN Center for Emergent Matter Science (CEMS), Wako 351-0198, Japan
[4] Research Center for Materials Nanoarchitectonics, National Institute for Materials Science, 1-1 Namiki, Tsukuba 305-0044, Japan

E-mail: yukishiomi@g.ecc.u-tokyo.ac.jp

Abstract. We have studied the Pockels effect, that is, the linear change in the refractive index of piezoelectric materials in response to an electric field, in monolayer and bilayer MoS_2 films grown by a chemical vapor deposition method. Optical imaging of the polarization rotation of the reflected light reveals that the polarization plane rotates by the application of an electric field only in monolayer MoS_2 which lacks inversion symmetry. The Pockels coefficient r_{22} is estimated to be -1.4 pm/V for monolayer MoS_2, which is comparable to the magnitude reported for GaAs.

1. Introduction

Since the groundbreaking work on graphene in 2004 [1], two-dimensional (2D) materials have been the focus of significant research efforts. 2D materials can be easily separated from adjacent layers that are weakly bonded by van der Waals forces, and atomically thin samples can be readily obtained just using adhesive tapes. Mechanical exfoliation is very simple, and the products are of high quality. However, each flake has a different number of layers that are randomly dispersed on the substrate, and the size is often small. Hence, various approaches have been developed for the preparation of 2D materials. One useful method is chemical vapor deposition (CVD), which enables the growth of large-scale 2D materials on various substrates [2, 3]. In addition to the tremendous number of material species in 2D materials [4], different atomically thin 2D materials can be stacked together by van der Waals forces to form 2D heterostructures. These atomic-layer 2D materials and 2D heterostructures display a rich variety of physical properties, which are promising for diverse applications [5, 6] such as electronics, photonics, optomechanics, and spintronics.

Besides graphene, widely studied are the family of transition metal dichalcogenides (TMDs) of the type MX_2, where M is a transition metal atom (Mo, W, etc.) and X is a chalcogen atom (S, Se, or Te) [7]. Unlike graphene which has no band gap, most TMDs are semiconductors that are ideal for electronic and photonic applications. The most well-known representative of TMDs is MoS_2. MoS_2 is a hexagonal crystal with layered structures

stacked by alternating S-Mo-S layers. In the bulk, MoS_2 is a semiconductor with an indirect band gap of $\sim$1.2 eV, but monolayer MoS_2 presents a direct band gap owing to quantum confinement [8, 9]. The direct band gap is suitable for efficient light applications, such as optoelectronics and nanophotonics. For example, ultrasensitive photodetectors based on MoS_2 have been developed [10]. TMDs are now considered important optical materials, since they are compatible with Si-based photonic devices and also provide additional value, *e.g.* mechanical flexibility, easy fabrication and integration, and robustness [11, 12].

The stacking degrees of freedom are another important property that modulates the physical properties of 2D materials. As to MoS_2, the electronic properties are largely modified by the number of layers and their stacking arrangement [13] because of variations in electronic and interlayer couplings. For example, the band gap in MoS_2 bilayer is altered by stacking as well as by several other means, such as strain [14, 15], sliding [16], and twisting [17]. Another important aspect of multilayers is the manipulation of symmetry breaking through stacking. This offers the possibility of manipulating the internal quantum degrees of freedom, such as spin, valley, and layer pseudospin in 2D materials, giving rise to exotic phenomena in spintronics, valleytronics, and twistronics [18]. Gate control of symmetry breaking was also demonstrated in bilayer MoS_2 [19, 20].

Symmetry breaking in materials is also essential in nonlinear optics which has developed into a key technology in condensed-matter physics, light generation, and quantum optics [21]. Nonlinear optical processes emerge from higher order expansion terms of polarization. Second-harmonic generation, sum- and difference frequency generation, optic rectification, and the Pockels effect are described by second-order nonlinear optical effects that are allowed in noncentrosymmetric crystals [22]. In the Pockels effect (or linear electro-optic effect), the application of a static electric field changes the refractive index of the materials. The Pockels effect can only occur in a material that lacks the center of inversion symmetry, and is thereby forbidden in centrosymmetric materials, except at their surfaces with broken inversion symmetry. Electro-optic modulation based on the Pockels effect which provides femto- or attoseconds response times [23] is one of the most fundamental applications of nonlinear optical materials, and serves a broad spectrum of applications, including telecommunications, quantum optics, optical computing, and biomedical imaging [24, 25, 26, 27, 28].

Though commercial nonlinear media are mainly bulk noncentrosymmetric crystals, TMDs and other 2D materials with low symmetry are considered promising materials for miniaturizing photonic and optoelectronic devices for on-chip integration [29] . Since TMDs with an odd number of layers can lack inversion symmetry as demonstrated by piezoelectric measurements [30, 31], second-order nonlinear optical effects are allowed that are not present in TMD crystals with an even number of layers. However, although the second-harmonic generation has been frequently used to characterize symmetry breaking [32], less attention has been paid to the Pockels effect in TMDs, to the best of our knowledge [11, 29, 33, 34]. In the present work, we experimentally study the Pockels effect for monolayer MoS_2 with a broken inversion symmetry at room temperature.

2. Methods

2.1. Experiments

Monolayer and bilayer MoS_2 lateral junctions were prepared on Si/SiO_2 substrates using a salt-assisted CVD method, as described previously [35]. For CVD growth, MoO_2 powders and S flakes were used as precursors and KBr powders were used as growth promoters. An optical image of the grown samples is shown in Fig. 1(a). Monolayer MoS_2 single crystals were grown in triangular shapes with lateral sizes over 30 μm. Triangular MoS_2 bilayer domains were found in the central part of the monolayer MoS_2. We obtained bilayer domains where MoS_2 triangles are stacked so that the vertices of each layer face in opposite directions, indicating a 2H-stacking configuration [36]. Since the 2H-stacked bilayer preserves the space inversion symmetry, the Pockels effect is forbidden for the bilayer domains, whereas it is allowed in the monolayer region lacking inversion symmetry. In/Au electrodes were fabricated on selected MoS_2 grains using maskless photolithography and resistive evaporation, as shown in Figs. 1(a) and (b).

Figure 1(c) shows the Raman spectra of monolayer and bilayer crystals excited by a 532 nm line in air ambient environment (LabRAM HR Evolution equipped with an EMCCD camera (HORIBA Scientific)). E_{2g} ($\sim$ 386-387 cm^{-1}) and A_{1g} ($\sim$ 406-407 cm^{-1}) modes were observed in both domains. For the bilayer domain, the frequency of E_{2g} peak decreases, whereas that of the A_{1g} peak increases from that of the monolayer domain. This thickness dependence is well consistent with the previous reports [37, 38].

To measure the Pockels effect, we used an optical system similar to the setup used for the polar magneto-optical Kerr effect [39, 40], which was constructed based on our previous paper [41]. A schematic drawing of the system is shown in Fig. 2(a). Linearly polarized laser light with a wavelength of 632.8 nm and power of 5 mW is focused at normal incidence onto the MoS_2 monolayer-bilayer crystals using a 100$\times$ microscope objective lens. The spot size is approximately 3 μm, and the position of the spot is scanned using an automatic stage to obtain a two-dimensional (2D) image. The reflected laser light is split by a Wollaston prism and detected by a balanced detector to analyze the polarization rotation. An ac electric field with a frequency of 1.563 kHz was applied along an in-plane direction of the sample, and the ac voltage signal from the balanced detector with the same frequency as that of the ac electric field was recorded using a lock-in amplifier. The polarization of the incident laser light is fixed in the electric-field direction. All the measurements were performed at room temperature. Gate voltage was not applied to MoS_2 in our measurements. The shift of the photoluminescence peak to a lower energy ($\sim$ 1.8 eV) (not shown) suggests that the MoS_2 crystals are clamped onto Si/SiO_2 substrates [42].

2.2. Analytical Model

Hereafter, the principal dielectric axes x_1, x_2, and x_3 in Fig. 1(b) are also denoted as x, y, and z, respectively. Owing to the Pockels effect, the refractive indices (second-rank tensor) n_i (i = 1-6) in low-symmetry semiconductors change from the principal refractive indices upon

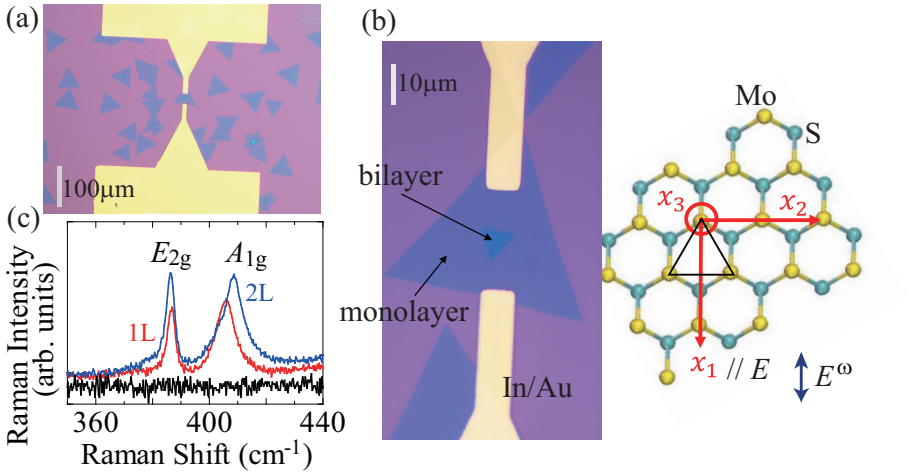

Figure 1. Monolayer and bilayer MoS_2 single crystals. (a) CVD-grown MoS_2 samples. Electrodes were fabricated for the selected samples. (b) Left: Optical image of a monolayer-bilayer MoS_2 film. The distance between the electrodes is set to 20-25 μm. Right: Crystal structure of MoS_2. x_1, x_2, and x_3 denote principal dielectric axes. Electric field (E) is applied almost parallel to the x_1 axis. E^ω denotes the polarization direction of the incident light. (c) Raman spectra of monolayer (1L) and bilayer (2L) MoS_2 domains. The black data represent background signals obtained from the substrate.

the application of the electric field E_j (j = 1-3). The Pockels effect is generally written as [43]

$$\Delta\left(\frac{1}{n_i}\right)^2 = \sum_{j=1}^{3} r_{ij}E_j. \tag{1}$$

Here, the change in the inverse permittivity tensor $\Delta(1/n_i^2)$ is expanded by the electric field, and the first order term of the electric field is the Pockels effect. r_{ij} are the Pockels coefficients and represented as a 6×3 matrix. Since the even-layer MoS_2 is centrosymmetric (point group of 6/mmm), all r_{ij} elements are zero. By contrast, the inversion symmetry of the odd-layer MoS_2 ($\bar{6}$m2) is broken, and r_{12}, r_{22}, and r_{61} can be nonzero. When we apply electric field E along the x_1 axis of MoS_2 [Fig. 1(b)], the change in the refrative index reads

$$\Delta\left(\frac{1}{n_6}\right)^2 = r_{61}E = -2r_{22}E. \tag{2}$$

For symmetry of $\bar{6}$m2, $r_{12} = -r_{22}$ and $r_{61} = -2r_{22}$ are expected.

The refractive index ellipsoid is then expressed as

$$\frac{x^2+y^2}{n_0^2} + \frac{z^2}{n_3^2} - 4r_{22}Exy = 1. \tag{3}$$

Here we used $n_1 = n_2 = n_0$ in the MoS_2 layer. When we use a new, rotated coordinate

$$x' = \frac{x-y}{\sqrt{2}},\ \ y' = \frac{x+y}{\sqrt{2}},\ \ z' = z, \tag{4}$$

the index ellipsoid becomes

$$\left(\frac{1}{n_0^2}-2r_{22}E\right)x'^2+\left(\frac{1}{n_0^2}+2r_{22}E\right)y'^2+\frac{z^2}{n_3^2}=1. \tag{5}$$

The x' and y' axes are the coordinate system rotated $-\pi/4$ around the z axis from the original x and y coordinate axes. Note that x', y', and z are the principal dielectric axes under an electric field applied along the x axis. The refractive indices modulated by the Pockels effect read

$$n_{x'}=n_0+n_0^3r_{22}E\equiv n_0+\Delta n \tag{6}$$

$$n_{y'}=n_0-n_0^3r_{22}E\equiv n_0-\Delta n \tag{7}$$

$$n_z=n_3. \tag{8}$$

In our experiment, the laser light with the linear polarization along the x (x_1) axis is irradiated from the z (x_3) axis. The electric-field dependence of $n_{x'}$ and $n_{y'}$ changes the linear polarization of the incident light to elliptical polarization, and also gives rise to the rotation of the polarization of the light. The oscillating electric field of the incident laser light is expressed in the (x', y') coordinate as

$$\boldsymbol{E}^i=(a\cos(\omega t-kz),\ a\cos(\omega t-kz)). \tag{9}$$

a, ω, t, and k are the amplitude, angular frequency, time, and wavenumber, respectively. Due to the Pockels effect, the amplitude and phase of the reflected light change from those of the incident light:

$$\boldsymbol{E}^r=(E_{x'},\ E_{y'})=(a_{x'}\cos(\omega t-kz+\delta_{x'}),\ a_{y'}\cos(\omega t-kz+\delta_{y'})), \tag{10}$$

where $a_{x'}\neq a_{y'}$ and $\delta_{x'}\neq\delta_{y'}$. Then we obtain

$$\left(\frac{E_{x'}}{a_{x'}}\right)^2+\left(\frac{E_{y'}}{a_{y'}}\right)^2-2\frac{E_{x'}}{a_{x'}}\frac{E_{y'}}{a_{y'}}\cos(\delta_{y'}-\delta_{x'})=\sin^2(\delta_{y'}-\delta_{x'}). \tag{11}$$

Hence, the reflected light has elliptical polarization. This equation can be transformed to the standard form equation of an ellipse in the α-rotated coordinate system from the (x',y') coordinate. α is determined by

$$\tan 2\alpha=\frac{2a_{x'}a_{y'}\cos(\delta_{y'}-\delta_{x'})}{a_{x'}^2-a_{y'}^2}. \tag{12}$$

When the modulation of the amplitudes due to the Pockels effect is small, *i.e.* $a_{x'},\ a_{y'}\approx a$, then $\alpha\approx\pi/4$.

According to the Fresnel equations, the amplitudes of the reflected light are

$$a_{x'}=\left(\frac{1-n_{x'}}{1+n_{x'}}\right)a\equiv r_{\perp x'}a,\ \ a_{y'}=\left(\frac{1-n_{y'}}{1+n_{y'}}\right)a\equiv r_{\perp y'}a. \tag{13}$$

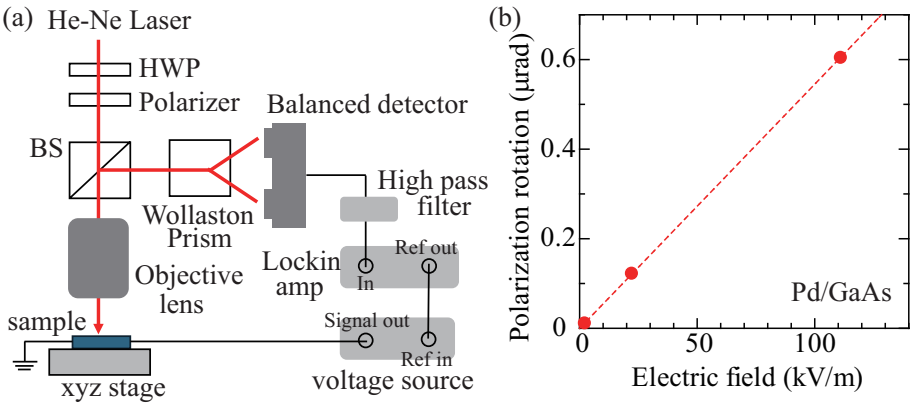

Figure 2. Measurement setup and test results. (a) Schematic diagram of the measurement setup for the polarization rotation due to the Pockels effect. HWP and BS denote the half-wave plate and the beam splitter, respectively. (b) Test results for the Pd/GaAs junction. Electric-field dependence of polarization rotation. The dotted line represents a linear fit.

We assume that the polarization rotation due to the Pockels effect $\Delta\alpha$ is small. Using the above relations and $\alpha = \pi/4 + \Delta\alpha$, we obtain

$$\Delta\alpha = \frac{1}{4}\left(\frac{r_{\perp y'}}{r_{\perp x'}} - \frac{r_{\perp x'}}{r_{\perp y'}}\right), \tag{14}$$

where $\delta_{y'} - \delta_{x'} \ll 1$ and $\Delta\alpha \ll 1$ were used. Using eqs.(6)-(8) and (13), $\Delta\alpha$ is expressed as

$$\Delta\alpha = \frac{2}{1-n_0^2}\Delta n = \frac{2n_0^3}{1-n_0^2} r_{22} E. \tag{15}$$

Here we used $\Delta n \ll 1$. Therefore, the polarization rotation due to the Pockels effect is proportional to the change in the refractive index Δn. $n_0 \approx 3.7$ was reported for monolayer MoS_2 at 632.8 nm [44]. By measuring electric-field dependence of $\Delta\alpha$, the Pockels coefficients can be estimated.

Note that the effect of multiple reflections at different interfaces (*e.g.*, Si/SiO_2 interface) and the interference effects resulting from these multiple reflections have been reported to be nontrivial [45]. Because the effects of multiple reflections were neglected in the magneto-optic Kerr effect measurement for monolayer CrI_3 [46], we have simplified the analytical model to a single reflection at the material interface.

3. Results and Discussion

First, we performed test measurements on GaAs, a typical noncentrosymmetric semiconductor. The point group of GaAs is $\bar{4}3m$, suggesting that $r_{41} = r_{52} = r_{63} (\neq 0)$ and all the other Pockels coefficients are zero. Also, initially $n_x = n_y = n_z = n_0$. When we apply the electric field along the z axis, the Pockels effect is expressed as

$$\Delta\left(\frac{1}{n_6}\right)^2 = r_{41} E. \tag{16}$$

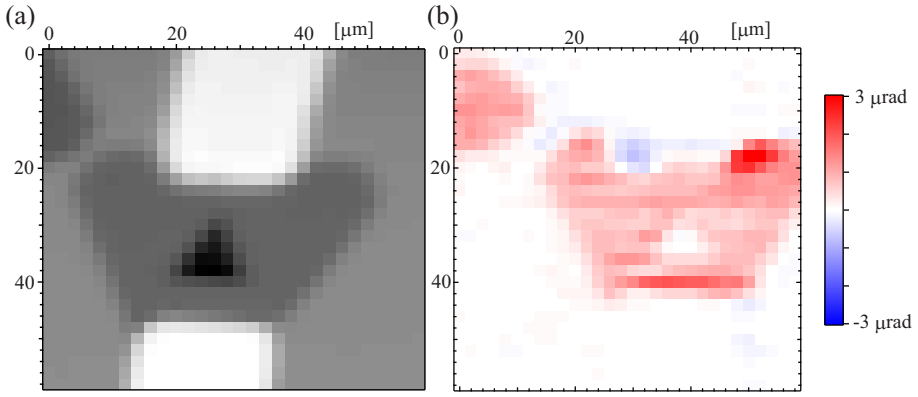

Figure 3. Polarization rotation due to the Pockels effect in monolayer and bilayer MoS_2 crystal. 2D mapping of (a) intensity of the reflected light and (b) polarization rotation for MoS_2 monolayer-bilayer sample. The applied voltage was set to 20 V. The electrode distance is 20 μm for this device.

The refractive index ellipsoid then becomes

$$\frac{x^2+y^2+z^2}{n_0^2}+2r_{41}Exy=1. \tag{17}$$

By the same procedure as in the previous section, we obtained

$$n_{x'}=n_0-\frac{1}{2}n_0^3r_{41}E \tag{18}$$

$$n_{y'}=n_0+\frac{1}{2}n_0^3r_{41}E \tag{19}$$

$$n_z=n_0. \tag{20}$$

These equations are similar to those in eqs.(6)-(8), and thus polarization rotation is also expected in GaAs.

The test sample is a commercially available undoped GaAs substrate with mirror surfaces. On the top surface that orients (001), thin Pd films were deposited at room temperature using a compact sputtering coater to apply an electric field to the metal/GaAs interface. The electrode distance is 450 μm. The laser light was irradiated from the [001] axis.

Figure 2(b) shows the electric-field dependence of the polarization rotation for Pd/GaAs. Polarization rotation was prominent around the Pd/GaAs interface, indicating that the voltage is concentrated near the interface. The averaged data over the region in which the signal was observed are plotted in Fig. 2(b). By linear fit in Fig. 2(b), we estimated $\Delta\alpha/E$ to be 5.4×10^{-12} rad m/V. Using $n_0=3.8$ [47], we obtain $r_{41}=-1.3$ pm/V. This value is close to the textbook value: -1.17 pm/V [48]. We have thereby judged that our measurement system provides reliable data.

We then measured the Pockels effect for the monolayer and bilayer MoS_2 crystals. During the measurement, we faced several problems; for example, some samples cracked

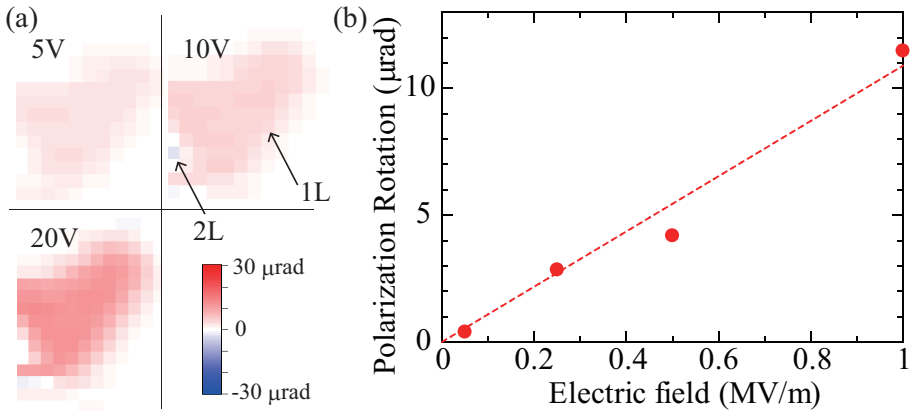

Figure 4. Electric-field dependence of polarization rotation in monolayer (1L) and bilayer (2L) MoS_2 crystal. (a) 2D mapping of the polarization rotation measured at different electric fields. (b) Electric-field dependence of the polarization rotation obtained from the experimental data shown in (a). The dotted line is a linear fit.

near the central portion by the application of a large electric field ($\sim$ 50 V). This is possibly attributed to the inverse piezoelectric effect, where the generated stress could overcome that from the substrate and produce strain. Nevertheless, we successfully observed a polarization rotation in response to an electric field in a relatively small voltage range ($\leq$ 20 V) for several MoS_2 samples, as shown in Fig. 3.

Figure 3 shows a 2D mapping of the intensity of the reflected laser light [Fig. 3(a)] and polarization rotation [Fig. 3(b)] measured at 1 MV/m for a monolayer-bilayer MoS_2 sample. As shown in Fig. 3(b), we observed polarization rotation in the entire monolayer area. In this measurement, the polarization rotation was approximately 3 μrad. Remarkably, the signal is less pronounced in the bilayer region; the polarization rotation is almost zero, as shown in Fig. 3(b). See Fig. 3(a) for the location of the bilayer domain. This result is consistent with the symmetry condition of the second-order nonlinear optical effects. The Pockels effect is active only in monolayer MoS_2 which lacks the inversion symmetry.

To estimate the Pockels coefficient in monolayer MoS_2, we subsequently performed systematic measurements under different electric fields, as shown in Fig. 4. Polarization rotation due to the Pockels effect is reproduced in this measurement, and the signals were observed in the entire monolayer regime. As shown in Fig. 4(a), the polarization rotation becomes larger monotonically with increasing electric field.

The magnitude of the polarization rotation is averaged over the area where the signal is visible, and plotted against the electric field in Fig. 4(b). An almost linear dependence is observed, as expected. Using a linear fit, the slope corresponding to $\Delta\alpha/E$ is estimated as 1.1×10^{-11} rad m/V. By using $n_0 \approx 3.7$ [44], eq.(15) yields $r_{22} = -1.4$ pm/V for the MoS_2 monolayer. Hence, the similar value of the Pockels coefficient to GaAs is obtained.

The Pockels effect for the MoS_2 monolayer was theoretically studied by M. Balaei *et al.* [49], and the second order of electrical conductivity related to the Pockels effect was calculated. From the real part of the permittivity calculated from the conductivity results, we have estimated Δn. Then, we roughly obtain a Pockels coefficient to be -0.8 pm/V. Here, we

assumed $n_0 \approx 3.7$ [44]. Our experimental results are thereby consistent with the theoretically estimated value.

The Pockels coefficients of inorganic bulk semiconductors are typically in the range of 1-10 pm/V [48]. For 2D materials, a first-principles calculation predicts that monolayer SnS exhibits a large Pockels effect with $r_{31} = -50$ pm/V [33]. Very recently, the Pockels effect was experimentally studied in $CuInP_2S_6$ flakes [34]. The out-of-plane Pockels coefficient was obtained as 20.28 pm/V. Compared with these results for other 2D materials, the Pockels coefficient of monolayer MoS_2 is not very large. However, our results show that the Pockels effect occurs even in the monolayer limit of TMD, and its magnitude is still comparable to the typical values reported for bulk crystals. These findings should be an important step toward the application of TMDs in nanoscale photonic and optoelectronic devices.

4. Conclusion

In summary, we experimentally demonstrated the Pockels effect for CVD-grown monolayer MoS_2, which is one of the most important 2D semiconductors for various applications. The measurement system was validated for a typical semiconductor GaAs prior to the measurements of MoS_2. From the polarization rotation in response to the applied electric field, the Pockels coefficient r_{22} was estimated as -1.4 pm/V for the MoS_2 monolayer. This value is comparable to that of typical semiconductors *e.g.* GaAs and ZnS, and consistent with the theoretically predicted value. The present results may constitute an important building block for realizing on-chip nonlinear optical devices based on 2D materials [50].

Based on these results, several important research directions are possible. First, the Pockels effect is also expected in other odd-layer MoS_2 crystals (three-layer, five-layer, etc.). It is therefore worthwhile to investigate the layer dependence of the Pockels effect. Because the second-order optical susceptibility decreases with increasing number of layers [51, 52], the Pockels coefficient could be smaller for thicker samples. We note that the piezoelectric effect for MoS_2 shows a similar tendency; the piezoelectric coefficient for trilayer MoS_2 samples is almost half that for monolayer MoS_2 [30].

Second, because the refractive index of MoS_2 depends on the wavelength of light, especially around the bandgap energy [53], future Pockels measurements for different wavelengths are important. It is notable that the monolayer MoS_2 bandgap was shown to be controlled by the dielectric environment [54]. Tunable Pockels cells could be realized using the bandgap modulation property of MoS_2 monolayer.

Acknowledgments

We thank Mr. Shotaro Yotsuya and Prof. Daisuke Kiriya for the Raman measurement, Mr. Shota Toida for the device fabrication support, Mr. Takahiko Endo for the CVD growth, and Prof. S. Fukatsu and Prof. S. Iguchi for the fruitful discussions. This work was supported by the Japan Science and Technology Agency (JST) FOREST Program, Grant No. JPMJFR203H and No. JPMJFR213X, and by the Japan Society for the Promotion of Science (JSPS)

KAKENHI, Grant No. JP21H05232, No. JP21H05234, No. JP22H04957, No. JP23K26525, No. JP24K21726, No. JP24H01177, and No. JP24K00566.

References

[1] K. S. Novoselov, A. K. Geim, S. V. Morozov, D. Jiang, Y. Zhang, S. V. Dubonos, I. V. Grigorieva, and A. A. Firsov. Electric field effect in atomically thin carbon films. Science, 306(5696):666–669, 2004.

[2] Hiroki Ago, Yui Ogawa, Masaharu Tsuji, Seigi Mizuno, and Hiroki Hibino. Catalytic growth of graphene: toward large-area single-crystalline graphene. The journal of physical chemistry letters, 3(16):2228–2236, 2012.

[3] Yifei Yu, Chun Li, Yi Liu, Liqin Su, Yong Zhang, and Linyou Cao. Controlled scalable synthesis of uniform, high-quality monolayer and few-layer mos_2 films. Scientific reports, 3(1):1866, 2013.

[4] Nicolas Mounet, Marco Gibertini, Philippe Schwaller, Davide Campi, Andrius Merkys, Antimo Marrazzo, Thibault Sohier, Ivano Eligio Castelli, Andrea Cepellotti, Giovanni Pizzi, et al. Two-dimensional materials from high-throughput computational exfoliation of experimentally known compounds. Nature nanotechnology, 13(3):246–252, 2018.

[5] Andrea C. Ferrari, Francesco Bonaccorso, Vladimir Fal'ko, Konstantin S. Novoselov, Stephan Roche, Peter Bøggild, Stefano Borini, Frank H. L. Koppens, Vincenzo Palermo, Nicola Pugno, José A. Garrido, Roman Sordan, Alberto Bianco, Laura Ballerini, Maurizio Prato, Elefterios Lidorikis, Jani Kivioja, Claudio Marinelli, Tapani Ryhänen, Alberto Morpurgo, Jonathan N. Coleman, Valeria Nicolosi, Luigi Colombo, Albert Fert, Mar Garcia-Hernandez, Adrian Bachtold, Grégory F. Schneider, Francisco Guinea, Cees Dekker, Matteo Barbone, Zhipei Sun, Costas Galiotis, Alexander N. Grigorenko, Gerasimos Konstantatos, Andras Kis, Mikhail Katsnelson, Lieven Vandersypen, Annick Loiseau, Vittorio Morandi, Daniel Neumaier, Emanuele Treossi, Vittorio Pellegrini, Marco Polini, Alessandro Tredicucci, Gareth M. Williams, Byung Hee Hong, Jong-Hyun Ahn, Jong Min Kim, Herbert Zirath, Bart J. van Wees, Herre van der Zant, Luigi Occhipinti, Andrea Di Matteo, Ian A. Kinloch, Thomas Seyller, Etienne Quesnel, Xinliang Feng, Ken Teo, Nalin Rupesinghe, Pertti Hakonen, Simon R. T. Neil, Quentin Tannock, Tomas Löfwander, and Jari Kinaret. Science and technology roadmap for graphene, related two-dimensional crystals, and hybrid systems. Nanoscale, 7:4598–4810, 2015.

[6] Hiroki Ago, Susumu Okada, Yasumitsu Miyata, Kazunari Matsuda, Mikito Koshino, Kosei Ueno, and Kosuke Nagashio and. Science of 2.5 dimensional materials: paradigm shift of materials science toward future social innovation. Science and Technology of Advanced Materials, 23(1):275–299, 2022. PMID: 35557511.

[7] Pablo Ares and Kostya S. Novoselov. Recent advances in graphene and other 2d materials. Nano Materials Science, 4(1):3–9, 2022. Special issue on Graphene and 2D Alternative Materials.

[8] Kin Fai Mak, Changgu Lee, James Hone, Jie Shan, and Tony F. Heinz. Atomically thin mos_2: A new direct-gap semiconductor. Phys. Rev. Lett., 105:136805, Sep 2010.

[9] Andrea Splendiani, Liang Sun, Yuanbo Zhang, Tianshu Li, Jonghwan Kim, Chi-Yung Chim, Giulia Galli, and Feng Wang. Emerging photoluminescence in monolayer mos_2. Nano letters, 10(4):1271–1275, 2010.

[10] Oriol Lopez-Sanchez, Dominik Lembke, Metin Kayci, Aleksandra Radenovic, and Andras Kis. Ultrasensitive photodetectors based on monolayer mos_2. Nature nanotechnology, 8(7):497–501, 2013.

[11] Zhipei Sun, Amos Martinez, and Feng Wang. Optical modulators with 2d layered materials. Nature Photonics, 10(4):227–238, 2016.

[12] Andrea C Ferrari, Francesco Bonaccorso, Vladimir Fal'Ko, Konstantin S Novoselov, Stephan Roche, Peter Bøggild, Stefano Borini, Frank HL Koppens, Vincenzo Palermo, Nicola Pugno, et al. Science and technology roadmap for graphene, related two-dimensional crystals, and hybrid systems. Nanoscale, 7(11):4598–4810, 2015.

[13] Natalia Cortés, Luis Rosales, Pedro A Orellana, Andrés Ayuela, and Jhon W González. Stacking change in mos2 bilayers induced by interstitial mo impurities. Scientific reports, 8(1):2143, 2018.

[14] Liang Dong, Avinash M Dongare, Raju R Namburu, Terrance P O'Regan, and Madan Dubey. Theoretical study on strain induced variations in electronic properties of 2h-mos_2 bilayer sheets. Applied Physics Letters, 104(5), 2014.

[15] Munish Sharma, Ashok Kumar, PK Ahluwalia, and Ravindra Pandey. Strain and electric field induced electronic properties of two-dimensional hybrid bilayers of transition-metal dichalcogenides. Journal of Applied Physics, 116(6), 2014.

[16] G Levita, A Cavaleiro, Elisa Molinari, T Polcar, and Maria Clelia Righi. Sliding properties of mos_2 layers: Load and interlayer orientation effects. The Journal of Physical Chemistry C, 118(25):13809–13816, 2014.

[17] Kaihui Liu, Liming Zhang, Ting Cao, Chenhao Jin, Diana Qiu, Qin Zhou, Alex Zettl, Peidong Yang, Steve G Louie, and Feng Wang. Evolution of interlayer coupling in twisted molybdenum disulfide bilayers. Nature communications, 5(1):4966, 2014.

[18] Luojun Du, Tawfique Hasan, Andres Castellanos-Gomez, Gui-Bin Liu, Yugui Yao, Chun Ning Lau, and Zhipei Sun. Engineering symmetry breaking in 2d layered materials. Nature Reviews Physics, 3(3):193–206, 2021.

[19] Julian Klein, Jakob Wierzbowski, Alexander Steinhoff, Matthias Florian, M Rosner, Florian Heimbach, K Muller, Frank Jahnke, Tim O Wehling, Jonathan J Finley, et al. Electric-field switchable second-harmonic generation in bilayer mos_2 by inversion symmetry breaking. Nano letters, 17(1):392–398, 2017.

[20] Jieun Lee, Kin Fai Mak, and Jie Shan. Electrical control of the valley hall effect in bilayer mos_2 transistors. Nature nanotechnology, 11(5):421–425, 2016.

[21] Linlin Zhou, Huange Fu, Ting Lv, Chengbo Wang, Hui Gao, Daqian Li, Leimin Deng, and Wei Xiong. Nonlinear optical characterization of 2d materials. Nanomaterials, 10(11):2263, 2020.

[22] Anton Autere, Henri Jussila, Yunyun Dai, Yadong Wang, Harri Lipsanen, and Zhipei Sun. Nonlinear optics with 2d layered materials. Advanced Materials, 30(24):1705963, 2018.

[23] M Thomaschewski and SI Bozhevolnyi. Pockels modulation in integrated nanophotonics. Applied Physics Reviews, 9(2), 2022.

[24] Guangcanlan Yang, Haochen Wang, Sai Mu, Hao Xie, Tyler Wang, Chengxing He, Mohan Shen, Mengxia Liu, Chris G Van de Walle, and Hong X Tang. Unveiling the pockels coefficient of ferroelectric nitride scaln. Nature Communications, 15(1):9538, 2024.

[25] Mohan Shen, Jiacheng Xie, Yuntao Xu, Sihao Wang, Risheng Cheng, Wei Fu, Yiyu Zhou, and Hong X Tang. Photonic link from single-flux-quantum circuits to room temperature. Nature Photonics, 18(4):371–378, 2024.

[26] Kai-Hong Luo, Sebastian Brauner, Christof Eigner, Polina R Sharapova, Raimund Ricken, Torsten Meier, Harald Herrmann, and Christine Silberhorn. Nonlinear integrated quantum electro-optic circuits. Science advances, 5(1):eaat1451, 2019.

[27] Prajnesh Kumar, Mingwei Jin, Ting Bu, Santosh Kumar, and Yu-Ping Huang. Efficient reservoir computing using field programmable gate array and electro-optic modulation. OSA Continuum, 4(3):1086–1098, 2021.

[28] Zhen Chen, BO Liu, Shengjie Wang, and Enhai Liu. Polarization-modulated three-dimensional imaging using a large-aperture electro-optic modulator. Applied Optics, 57(27):7750–7757, 2018.

[29] Xinglin Wen, Zibo Gong, and Dehui Li. Nonlinear optics of two-dimensional transition metal dichalcogenides. InfoMat, 1(3):317–337, 2019.

[30] Hanyu Zhu, Yuan Wang, Jun Xiao, Ming Liu, Shaomin Xiong, Zi Jing Wong, Ziliang Ye, Yu Ye, Xiaobo Yin, and Xiang Zhang. Observation of piezoelectricity in free-standing monolayer mos2. Nature nanotechnology, 10(2):151–155, 2015.

[31] Wenzhuo Wu, Lei Wang, Yilei Li, Fan Zhang, Long Lin, Simiao Niu, Daniel Chenet, Xian Zhang, Yufeng Hao, Tony F Heinz, et al. Piezoelectricity of single-atomic-layer mos2 for energy conversion and piezotronics. Nature, 514(7523):470–474, 2014.

[32] Yilei Li, Yi Rao, Kin Fai Mak, Yumeng You, Shuyuan Wang, Cory R Dean, and Tony F Heinz. Probing symmetry properties of few-layer mos_2 and h-bn by optical second-harmonic generation. Nano letters,

13(7):3329–3333, 2013.

[33] Zhijun Jiang, Charles Paillard, Hugh O. H. Churchill, Minggang Xia, Shengli Zhang, Hongjun Xiang, and L. Bellaiche. Large linear and nonlinear electro-optic coefficients in two-dimensional ferroelectrics. Phys. Rev. B, 106:L081404, Aug 2022.

[34] Yuanda Liu, Yaze Wu, Ruihuan Duan, Jichao Fu, Martin Ovesen, Samuel Chang En Lai, Think-E Yeo, Jing Yee Chee, Yunjie Chen, Siew Lang Teo, et al. Linear electro-optic effect in 2d ferroelectric for electrically tunable metalens. Advanced Materials, 36(29):2401838, 2024.

[35] Naoki Wada, Jiang Pu, Yuhei Takaguchi, Wenjin Zhang, Zheng Liu, Takahiko Endo, Toshifumi Irisawa, Kazunari Matsuda, Yuhei Miyauchi, Taishi Takenobu, and Yasumitsu Miyata. Efficient and chiral electroluminescence from in-plane heterostructure of transition metal dichalcogenide monolayers. Advanced Functional Materials, 32(40):2203602, 2022.

[36] Xuefei Li, Xinhang Shi, Damiano Marian, David Soriano, Teresa Cusati, Giuseppe Iannaccone, Gianluca Fiori, Qi Guo, Wenjie Zhao, and Yanqing Wu. Rhombohedral-stacked bilayer transition metal dichalcogenides for high-performance atomically thin cmos devices. Science Advances, 9(7):eade5706, 2023.

[37] Shengxi Huang, Liangbo Liang, Xi Ling, Alexander A Puretzky, David B Geohegan, Bobby G Sumpter, Jing Kong, Vincent Meunier, and Mildred S Dresselhaus. Low-frequency interlayer raman modes to probe interface of twisted bilayer mos_2. Nano letters, 16(2):1435–1444, 2016.

[38] Hong Li, Qing Zhang, Chin Chong Ray Yap, Beng Kang Tay, Teo Hang Tong Edwin, Aurelien Olivier, and Dominique Baillargeat. From bulk to monolayer mos_2: evolution of raman scattering. Advanced Functional Materials, 22(7):1385–1390, 2012.

[39] Wenrui Wang, Tao Wang, Vivek P Amin, Yang Wang, Anil Radhakrishnan, Angie Davidson, Shane R Allen, Thomas J Silva, Hendrik Ohldag, Davor Balzar, et al. Anomalous spin–orbit torques in magnetic single-layer films. Nature nanotechnology, 14(9):819–824, 2019.

[40] Christian Stamm, Christoph Murer, Marco Berritta, Junxiao Feng, Mihai Gabureac, Peter M Oppeneer, and Pietro Gambardella. Magneto-optical detection of the spin hall effect in pt and w thin films. Physical review letters, 119(8):087203, 2017.

[41] T. Yokouchi and Y. Shiomi. Enhancement of current-induced out-of-plane spin polarization by heavy-metal-impurity doping in Fe thin films. Phys. Rev. Appl., 16:054001, Nov 2021.

[42] P. Günter and M. Zgonik. Clamped–unclamped electro-optic coefficient dilemma in photorefractive phenomena. Opt. Lett., 16(23):1826–1828, Dec 1991.

[43] Robert W Boyd. Nonlinear Optics. Academic Press, March 2008.

[44] Kazi M Islam, Ron Synowicki, Timothy Ismael, Isaac Oguntoye, Nathan Grinalds, and Matthew D Escarra. In-plane and out-of-plane optical properties of monolayer, few-layer, and thin-film mos_2 from 190 to 1700 nm and their application in photonic device design. Advanced photonics research, 2(5):2000180, 2021.

[45] Kobe De Geest, Enes Lievens, Ewout Picavet, Klaartje De Buysser, Dries Van Thourhout, and Jeroen Beeckman. Extraction of individual pockels coefficients of thin films via interferometric reflection measurements. Journal of Physics: Photonics, 7(1):015012, 2025.

[46] Bevin Huang, Genevieve Clark, Efrén Navarro-Moratalla, Dahlia R Klein, Ran Cheng, Kyle L Seyler, Ding Zhong, Emma Schmidgall, Michael A McGuire, David H Cobden, et al. Layer-dependent ferromagnetism in a van der waals crystal down to the monolayer limit. Nature, 546(7657):270–273, 2017.

[47] D. E. Aspnes, S. M. Kelso, R. A. Logan, and R. Bhat. Optical properties of $al_xga_{1-x}as$. Journal of Applied Physics, 60(2):754–767, 07 1986.

[48] Kazuo KURODA. Electrooptic and nonlinear optical materials and devices i. The Review of Laser Engineering, 28(8):548–555, 2000.

[49] Mohsen Balaei, Rouhollah Karimzadeh, and Tayebeh Naseri. Introducing a novel approach to linear and nonlinear electrical conductivity of mos_2. Optical Materials Express, 11(8):2665–2674, 2021.

[50] Vincent Pelgrin, Hoon Hahn Yoon, Eric Cassan, and Zhipei Sun. Hybrid integration of 2d materials for on-chip nonlinear photonics. Light: Advanced Manufacturing, 4(3):311–333, 2023.

[51] Nardeep Kumar, Sina Najmaei, Qiannan Cui, Frank Ceballos, Pulickel M. Ajayan, Jun Lou, and Hui Zhao. Second harmonic microscopy of monolayer mos_2. Phys. Rev. B, 87:161403, Apr 2013.

[52] Chung-Yu Wang and Guang-Yu Guo. Nonlinear optical properties of transition-metal dichalcogenide mx2 (m = mo, w; x = s, se) monolayers and trilayers from first-principles calculations. The Journal of Physical Chemistry C, 119(23):13268–13276, 2015.

[53] Georgy A Ermolaev, Yury V Stebunov, Andrey A Vyshnevyy, Dmitry E Tatarkin, Dmitry I Yakubovsky, Sergey M Novikov, Denis G Baranov, Timur Shegai, Alexey Y Nikitin, Aleksey V Arsenin, et al. Broadband optical properties of monolayer and bulk mos2. npj 2D Materials and Applications, 4(1):21, 2020.

[54] Junga Ryou, Yong-Sung Kim, Santosh Kc, and Kyeongjae Cho. Monolayer mos2 bandgap modulation by dielectric environments and tunable bandgap transistors. Scientific reports, 6(1):29184, 2016.